Date 2012
Author Li, Ziru and Tom van Terwisga

Address Delft University of Technology
Ship Hydromechanics and Structures Laboratory
Mekelweg 2, 2628 CD Delft

TUDelft

Delft University of Technology

On the capability of a RANS method to assess the cavitation erosion risk on a hydrofoil.

by

Li, Ziru and Tom van Terwisga.

Report No. 1887-P 2012

Proceedings of the International Symposium on Cavitation, CAV2012, 13-16 August 2012, Singapore, ISBN: 978-981-07-2826-7.

Proceedings of the

8th International Symposium on Cavitation

13 – 16 August 2012
Singapore

ISBN: 978-981-07-2826-7

Editors
Claus-Dieter Ohl, Evert Klaseboer, Siew Wan Ohl, Shi Wei Gong and B. C. Khoo

Published by
RESEARCH PUBLISHING

Hosted by
Institute of High Performance Computing
NANYANG TECHNOLOGICAL UNIVERSITY
NUS National University of Singapore

Sponsors
Dynamic
ZUGO
Newport
CAD
Springer
NANYANG TECHNOLOGICAL UNIVERSITY
Lam RESEARCH

Bubbly Flows and Cloud Cavitation

BACK

Numerical

- Development of a Nonlinear Asymptotic Method for Calculation of Nearly Axisymmetric Cavitation Flows
  V. N. Buyvol and V. V. Serebryakov

- Efficient Numerical Simulation of Unsteady Cavitating Flows Using Thermodynamic Tables
  F. Khatami, A. H. Koop, E. T. A. van der Weide and H. W. M. Hoeijmakers

- Evaluation of Cavitation Models for Prediction of Transient Cavitating Flows around a Stationary and a Pitching Hydrofoil
  Biao Huang, Antoine Ducoin and Yin Lu Young

- Features of Nucleation and Growth of Gas Bubbles in Magmas
  Davydov Maxim

- Further Improvement of Bubble Model for Cavitating Flow Simulations
  Yoshiaki Tamura, Nobuo Tsurumi and Yoichiro Matsumoto

- Growth and Collapse of Laser Generated Bubbles Near a Curved Density Interface
  Mark Esson

- MGFM Applied to Underwater Explosion near a Thin Plate with Cavitation Evolution
  Liu Tiegang, Feng Chengliang and Xu Liang

- Modeling Cavitation Flow of Cryogenic Fluids with Thermodynamical Phase-Change Theories
  Zhang XiaBin, Wei Zhang and Qiu LiMim

- Modelling the Total Monomeric Anthocyanin (TMA) Extracted From Mangosteen Hull in Ultrasonic Assisted Acidified Aqueous Solvent Extractions
  C. Y. Cheok N. L. Chin, Y. A. Yusof, R. A. Talib and C. L. Law

- MTBE-Degradation by Hydrodynamic Induced Cavitation
  Andreas Schmid

- Non-Singular Boundary Integral Method and Its Applications to Oscillating Bubbles
  Qiang Sun, Evert Klaseboer, Boo Cheong Khoo and Derek Y. C. Chan

- Numerical Analysis for Influence of Cascade Solidity on the Performances of Cavitating Inducers
  Li Xiaojun, Yuan Shouqi, Pan Xiwei and Pan Zhongyong

- Numerical Analysis for Influence of Cascade Solidity on the Performances of Cavitating Inducers
  Li Xiaojun, Yuan Shouqi, Pan Xiwei and Pan Zhongyong

- Numerical Analysis of Axisymmetric Supercavitating Flows
  Byoung-Kwon Ahn, Hyun-Gil Jang, Hyoung-Tae Kim and Chang-Sup Lee

- Numerical Investigations of Nonspherical Bubble Collapse Near Boundaries by the Improved Ghost Fluid Method
  Yoshinori Jinbo, Toshiyuki Ogasawara and Hiroyuki Takahira

- Numerical Method for the Analysis of Cavitating Waterjet Propulsion Systems
  Shu-Hao Chang and Spyros A. Kinnas

- Numerical Simulation and Analysis of Cavitating Flow in a Centrifugal Pump
  Dongxi Liu, Houlin Liu, Yong Wang, Suguo Zhuang, Jian Wang and Du Hui

- Numerical Simulation of Cavitation around a Two-Dimensional Hydrofoil using VOF Method and LES Turbulence Model
  Ehsan Roohi, Amir Pouyan Zahiri and Mahmud Pasandideh-Fard

- Numerical Simulation of Cavitation Flow Around a Hydrofoil
  Houlin Liu Jian Wang, Bixing Yin, Yong Wang, Suguo Zhuang and Dongxi Liu

- On the Capability of a RANS Method to Assess the Cavitation Erosion Risk on a Hydrofoil
  Ziru Li and Tom Van Terwisga

- Performance Assessments for Various Numerical Cavitation Models using Experimental Data
  Yaw-Huei Lee, Jing-Chin Tu, Yu-Chi Chang and Yi-Chih Chow

- Periodic Phenomena on a Partially Cavitating Hydrofoil
  Anne Gosset, Marcos Lema and Fernando López Peña

- Phase Change Model based on the Idea of Apparent Phase Equilibrium in Unsteady Cavitating Flow
  Yuka Iga

- Prediction of Cavitation on Two- and Three-Dimensional Hydrofoils by an Iterative BEM
  Yasemin Arikan, Fahri Çelik, Ali DoĞrul and Şakir Bal

Measurements

Proceedings of the 8th International Symposium on Cavitation
CAV2012 – Abstract No. 113
August 14-16, 2012, Singapore

On the capability of a RANS method to assess the cavitation erosion risk on a hydrofoil

Ziru Li
Delft University of Technology, The Netherlands
Wuhan University of Technology, China

Tom Van Terwisga
Delft University of Technology, The Netherlands
Maritime Research Institute Netherlands (MARIN)

SUMMARY

This paper aims at an assessment of the cavitation erosion risk by using a contemporary unsteady RANS method in conjunction with post-processing procedures, without the necessity to compute the details of the actual collapses. Such a procedure is developed from detailed investigations on the flow over hydrofoils.

The first objective is to get a better understanding of the unsteady cavitation dynamics over hydrofoils and the physics that may lead to a high risk of cavitation erosion. The capability of the multiphase RANS method to predict the relevant and critical unsteady cavitation dynamics is examined on a NACA0015 hydrofoil. It is found that the large-scale structures and typical unsteady cavitation dynamics predicted by the RANS method are in fair agreement with the experimental observations.

The second objective is to find a methodology for the assessment of the risk of cavitation erosion on the surface of hydrofoils by using unsteady RANS simulations as input. A new erosion intensity function is proposed based on the mean value of the time derivative of the local pressure that exceeds a certain threshold. The evaluation on a NACA0015 hydrofoil shows that a good correlation is found between the locations with a computed high erosion risk and the damage area observed from paint tests.

INTRODUCTION

A cavitating flow is a complicated multiphase flow involving phase change, compressibility, viscous effects and turbulent fluctuations. Cavitation will occur in the regions where the pressure is lower than a critical value, always related to the vapor pressure. It is a common phenomenon that often occurs in the flow over propulsion systems, rudders and other hydraulic machinery.

Due to the limitations imposed on the attainable propulsor thrust and efficiency by cavitation induced vibrations and cavitation erosion risk, it becomes essential to predict cavitation and assess cavitation hindrance in an early design stage. Among all adverse effects of cavitation, cavitation erosion is the most complex since it involves multi-scale hydrodynamic processes combined with the response of solid material which is exposed to the cavitating flow. Predicting the quantitative cavitation aggressiveness and the most likely location of cavitation erosion are complex problems that have motivated an important amount of basic and applied research in the fields of hydrodynamics, mechanical engineering and metallurgy. From an industrial point of view, the evaluation of the erosion power of cavitating flows and prediction of the material damage remains a major concern for both the design and maintenance stage.

A wide range of studies that deal with problems from bubble dynamics to material testing have been made, all aiming toward a deeper understanding of these phenomena. Recently, a number of attempts to predict the cavitation erosion risk were published (e.g. Fortes-Patella et al, 2004 [1]; Dular et al, 2006 [2]; Nohmi et al, 2008 [3]) with the aid of visual observations and CFD tools. Although much is known about the individual bubble dynamics and the material reaction, no reliable theoretical prediction methods for cavitation erosion, which involve all elements of cavitation erosion, has so far been made successfully. It is still a big challenge to numerically predict the risk of cavitation erosion without the support of model tests.

Van Terwisga et al. (2009) [4] hypothesized that the erosive action by cavitation is largely caused by the acoustic shock waves that are released upon collapse of a focused cavity. This hypothesis builds further on the fundamental work done on cavitation erosion by Bark et al. (2004) [5]. It is suggested here that the focusing of potential energy in the cavity is occurring through large scale vortices occurring in the break-up region of sheet cavitation. This paper focuses on the question whether the conditions for erosive cavitation can be predicted from an unsteady RANS method, without the necessity to compute the details of the actual collapse. This would then justify a focus on modeling efforts of essentially the large scale cavity dynamics only.

At first, the capability of the multiphase RANS method to predict the unsteady cavitation dynamics is initially explored through simulations of the cavitating flow over a NACA0015 hydrofoil at an 8° angle of attack. With the RANS method

implemented in FLUENT, the break-up of the sheet cavity and also the periodic shedding of the cloud cavity at the trailing edge of the sheet can however only be predicted by an artificial reduction of the turbulent viscosity in the regions of higher vapor volume fraction as suggested by Reboud et al. (1998) [6]. It is noted that other RANS codes such as Star-CD (Oprea, 2009 [7]) and FreSCo (Hoekstra and Vaz, 2008 [8]) do not need this viscous correction. However, for the Delft Twist-11 Hydrofoil used as a common test case in the SMP2011workshop (Hoekstra et al., 2011 [9]), only steady or at most a breathing behavior was observed by all the participants applying a RANS method, where unsteady dynamics was actually observed in the experiments. The simulation results for the NACA0015 hydrofoil at $8°$ angle of attack are then compared with experimental results from the MARIN High Speed Cavitation Tunnel (Van Rijsbergen and Boorsma, 2011 [10]).

The qualitative correlation between the risk of cavitation erosion and unsteady cavitation phenomena has been investigated by post-processing the RANS results for this NACA0015 hydrofoil test case. Among several criteria suggested by an analysis of the potential power that is stored in the vapor structure, the time derivate of the local pressure, $\partial p / \partial t$, shows best correlation with the observed damaged areas [17]. A new erosion function is finally presented based on the mean value of $\partial p / \partial t$ values that exceed a certain threshold. A good correlation has been found between the thus predicted locations with high erosion risk and the damaged area observed from the paint tests.

NUMERICAL MODELS

Governing Equations

The governing equations for a two-phase flow are based on a single-fluid approach, regarding the mixture as one liquid. The flow field is solved for the mixture continuity and momentum equations:

$$\frac{\partial}{\partial t}(\rho_m) + \nabla \cdot (\rho_m \vec{u}) = 0 \tag{1}$$

$$\frac{\partial}{\partial t}(\rho_m \vec{v}) + \nabla \cdot (\rho_m \vec{u}\vec{u}) = -\nabla p + \nabla \cdot [\mu_m (\nabla \vec{u} + \nabla \vec{u}^T)] + \rho_m \vec{g} + \vec{F} \tag{2}$$

Here the relationship between the mixture density ρ_m and the vapor volume fraction α is defined as:

$$\rho_m = \alpha \rho_v + (1-\alpha)\rho_l \tag{3}$$

where the subscripts m, v and l represent mixture, vapor and liquid phase respectively.

Turbulence Modeling

The *SST* $k-\omega$ turbulence model developed by Menter (2004) [11] is adopted in this study, which is a blending between the $k-\omega$ model in the near-wall region and the $k-\varepsilon$ model in the far field. The refinements of the $k-\omega$ model and a blending function can make this model behave properly in both the near-wall and far-field zones.

To improve the cavity dynamics in the simulation, a modification of the turbulent viscosity, μ_t, is applied following the idea of Reboud et al. (1998) [6]:

$$\mu_t = f(\rho) C_\omega \frac{k}{\omega} \tag{4}$$

$$f(\rho) = \rho_v + \frac{(\rho_m - \rho_v)^n}{(\rho_l - \rho_v)^{n-1}}; \quad n \gg 1 \tag{5}$$

With a recommended exponent value $n = 10$, the turbulent viscosity in the region with higher vapor volume fraction is reduced to better simulate the re-entrant jet and shedding behavior.

Cavitation Modeling

The cavitation model adopted here is developed by Schnerr & Sauer. The transport equation for the vapor volume fraction has the general form:

$$\frac{\partial}{\partial t}(\alpha \rho_v) + \nabla \cdot (\alpha \rho_v \vec{u}) = S_e - S_c \tag{6}$$

where the source terms R_e and R_c refer to the evaporation and condensation of the vapor bubbles respectively, accounting for the mass transfer between the vapor and liquid phases in cavitation.

The source terms are derived from the Rayleigh-Plesset equation and are defined as:

$$S_e = \frac{\rho_v \rho_l}{\rho_m} \alpha (1-\alpha) \frac{3}{R} \sqrt{\frac{2}{3} \frac{(p_v - p)}{\rho_l}}, \text{ when } p_v \geq p \tag{7}$$

$$S_c = \frac{\rho_v \rho_l}{\rho_m} \alpha (1-\alpha) \frac{3}{R} \sqrt{\frac{2}{3} \frac{(p - p_v)}{\rho_l}}, \text{ when } p_v \leq p \tag{8}$$

The bubble radius can be related to the vapor volume fraction α and the bubble number density n_b as follows:

$$R = \left(\frac{\alpha}{1-\alpha} \frac{3}{4\pi n_b}\right)^{\frac{1}{3}} \tag{9}$$

where n_b is the only parameter to be provided as input for FLUENT with a default value of $1e+13$.

CASE DESCRIPTION

The test geometry is a NACA0015 hydrofoil at $8°$ angle of attack with a chord length $C = 60mm$. The three-dimensional characteristics of the unsteady cavitating flow over this hydrofoil are examined by extruding the 2D geometry in the span-wise direction by half of the width of the hydrofoil, i.e. $20mm$.

In chord-wise direction, a multiblock topology is adopted, consisting of an O-grid around the foil embedded in an H-grid (12 blocks). The computational domain extends 3.0 chord-lengths ahead of the leading edge, and 5.5 chord-lengths behind the trailing edge of the hydrofoil. 264 edges are set on the hydrofoil, such that the near-wall mesh resolution along the hydrofoil surface is $y^+ < 1$.

The unsteady dynamics is then investigated on a specific cavitation regime for a cavitation number of $\sigma = 2.01$. A velocity-inlet condition is applied in the upstream inlet plane with the vapor volume fraction equal to zero. A pressure outlet condition is used at the outlet plane. The specified pressure at the outlet can be derived from the cavitation number. On the tunnel walls, a no-slip wall condition is applied whereas a symmetry condition is applied on the mid-span. The physical

properties of the two-phases, liquid and vapor, are taken at a temperature of $16.3°C$. The detailed initial and boundary conditions and the flow properties are listed in Table 1.

Table 1: Boundary conditions and flow properties for a NACA0015 hydrofoil at $8°$ angle of attack

Boundary Conditions	NACA0015 (AoA=8°)	
Velocity Inlet (m/s)	V=17.3	
Pressure Outlet(kPa)	302.295	
Tubulent Intensity (%)	1	
Tubulent Viscosity Ratio	10	
Foil	No-slip Wall	
Mid-span	Symmetry	
Tunnel Walls	No-slip Wall	
Flow Properties (T=16.3°C)	Vapor	Liquid
Density (kg/m3)	0.01389	998.85
Dynamic Viscosity(kg/ms)	9.63E-06	0.0011
Vapor Pressure (kPa)	1.854	

A fully coupled solver is used to solve the pressure and momentum equations, which can lead to a more robust calculation and faster convergence [12]. The pressure is discretized using the PRESTO! scheme, and the convection term of the momentum equations are discretized by the QUICK scheme. The same is done for the terms in the turbulence equations and vapor volume fraction equation.

The experiments to be compared with the numerical simulations are performed by MARIN in cooperation with Lloyd's Register [10]. The test conditions for the selected case (Run No. 26) resemble the conditions in the simulation by the RANS method, as listed in Table 2.

Table 2: Test conditions for Run No. 26

	Run No. 26
AoA (deg)	8
V(m/s)	17.3
σv	2.01
Re	9.50E+05

NUMERICAL RESULTS

The RANS results with the modified $SST\ k-\omega$ turbulence model basically reproduce the features of the shedding process observed in the cavitation tunnel at the selected test condition, such as the detachment of the cloudy cavities from the main sheet cavity and the collapse of the cloudy cavities. The time history of the volume integral of the vapor volume fraction shows a high-frequency fluctuation ($f \approx 216Hz$) together with an unsteady amplitude characterized by a very low frequency ($f \approx 36Hz$). It is qualitatively similar as to what has been observed in the 2D computation domain [13].

Typical images obtained by visualizing the iso-surface of the instantaneous vapor fraction defined by $\alpha = 0.1$ in top view and downstream view are separately shown in Figure 1, representing a typical shedding cycle at the high frequency. The observed unsteady phenomena can be characterized as follows:

- The leading edge sheet cavity is growing together with the collapse of the cloudy cavity formed from the last pinch-off (Figure 1-①);
- Re-entrant flow moves upstream towards to the leading edge until it breaks the main sheet cavity. The upstream part of the sheet cavity partially disappears from the mid-span (Figure 1-②);
- The downstream part of the sheet cavity starts to roll up from the foil surface and forms a cloudy cavity in a cylindrical shape, slightly thicker at the mid-span and thinner at the sides of the hydrofoil (Figure 1- ③);
- The remaining upstream part of the main sheet cavity prolongs in span-wise location, and is subsequently merged into the new sheet cavity that develops from the leading edge again. The cloudy cavity downstream gradually transforms into a horse-shoe shape (Figure 1- ④⑤);
- Finally, the cloud cavity collapses downstream and the leading edge sheet cavity extends along the chord length, initiating a new cycle (Figure 1- ⑥).

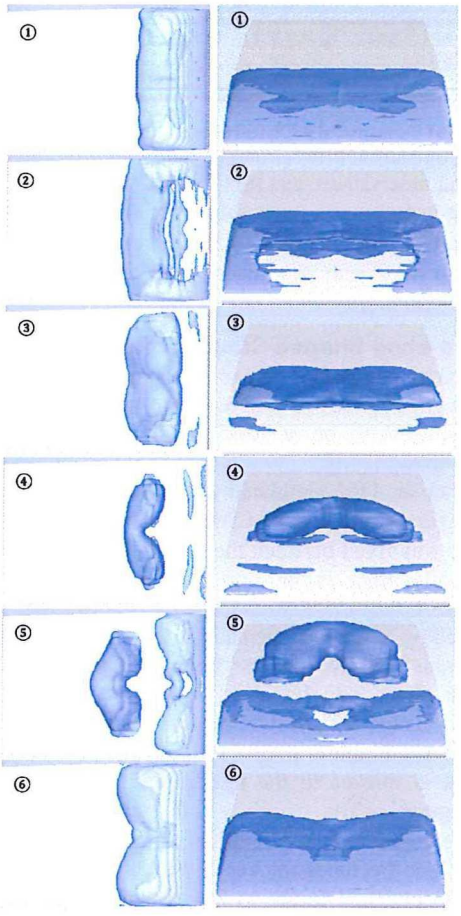

(a) Top view (b) Downstream view

Figure 1: Sequences of iso-surface plots of the instantaneous vapor volume fraction of $\alpha = 0.1$ during one typical shedding cycle in (a) top view (Flow from right to left); and (b) downstream view on the NACA0015 hydrofoil (3D representation) at $8°$ angle of attack at $\sigma = 2.01$ with the modified $SST\ k-\omega$ turbulence model

When comparing the numerical simulation results with the experimental observations, it is found that the synchronization of the collapse of the cloudy cavities and the development and break-up of the leading edge sheet cavity is a bit different but qualitatively shows a good match, as shown in Figure 2.

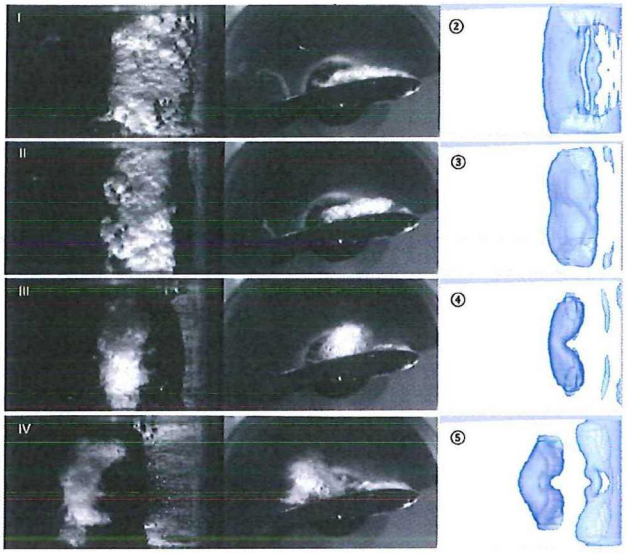

(a) Experimental Observations (b) Numerical Simulations

Figure 2: Comparison between several typical instants obtained by (a) experimental observations; and (b) numerical simulations (iso-surface plots of the instantaneous vapor volume fraction of $\alpha = 0.1$) for the flow over a NACA0015 hydrofoil (3D representation) at 8° angle of attack at $\sigma = 2.01$ with the modified $SST\ k-\omega$ turbulence model (Flow from right to left)

Horse-shoe Shaped Cloudy Cavity

A typical horse-shoe vapor structure has been observed during the experiments as well as in the numerical simulations. It is considered to be at least one driving mechanism for cavitation erosion [14].

Saito et al. [15] simulated a three-dimensional unsteady cavitating flow around a NACA0015 hydrofoil at 8° angle of attack that was fixed between the sidewalls, and explained that the sidewall effect is an important factor in causing the generation of the horse-shoe shaped cloudy cavity, which is also noticed by Van Rijsbergen and Boorsma (2011) [10].

The transformation process from a cylindrical shape into a horse-shoe shape can be clearly observed during a typical shedding cycle (see Figure 1). It can be described as follows:

- The shed cavity at first rolls up in a cylindrical shape that is thicker in the middle and thinner at the sides (Figure 1- ③);
- The center of this cylindrical cloudy cavity is then lifted up, and becomes thicker and thicker, however its sides keep attached to the hydrofoil surface. This "head" of the cloudy cavity will be dragged further downstream than the "legs" that are attached to the surface (Figure 1- ④);
- The "head" is lifted even higher and dragged even further downstream, and the "legs" move towards the mid-span (Figure 1-⑤). The cylindrical cloudy cavity then finally develops into a horse-shoe shape or U-shape structure.

Three stages of a typical horse-shoe shaped cloudy cavity from break-off to violent collapse were sketched by Kawanami et al. (2002) [14], as shown in Figure 3. The bubbles contained in the cavity seem to get attracted toward the foil surface possibly by vortex stretching of the legs in the viscous boundary layer over the foil, and the horse-shoe cavity is thereby split at the head. Then the remaining two legs of the horse-shoe cavity collapse toward the foil surface, potentially causing local cavitation erosion.

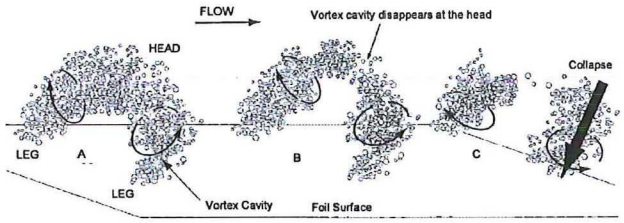

Figure 3: Schematic diagram of the transformation process of a horse-shoe cloudy cavity from break-off to violent collapse (Kawanami et al.[12])

It is also observed by Van Rijsbergen and Boorsma (2011) [10] that the middle part of the cloud implodes and leaves two separate vortices on both sides of the foil. A comparison between the numerical results and the experimental observations is shown in Figure 4.

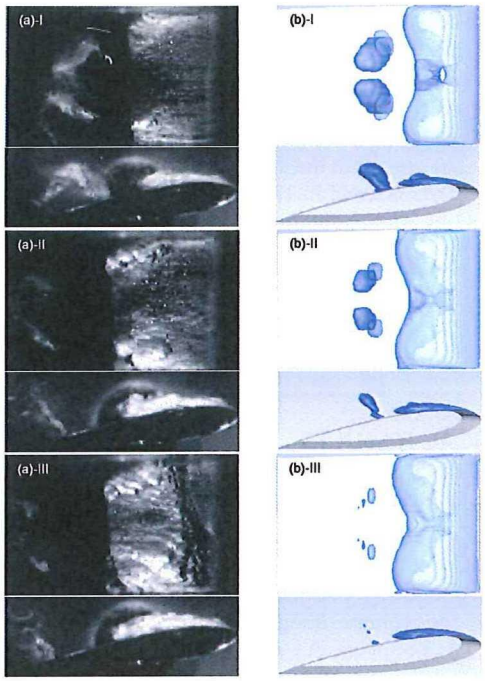

(a) Experimental Observations (b) Numerical Simulations

Figure 4: Comparison of three typical instants during the collapse of the horse-shoe shaped cloudy cavity between the (a) Experimental observations; and (b) Numerical results using the current approach (Flow from right to left)

It can be observed that the basic features of the collapse process have been captured by the current RANS method, such as the collapse of the horse-shoe cloudy cavity into two vortex structures on both sides and the shrinking and collapse of the remaining part toward the foil surface. However, Van Rijsbergen and Boorsma (2011) [10] observed that the downstream attachment of the two legs of the horse-shoe

shaped cloudy cavity was located further aftward than in the numerical prediction. Furthermore, the vortices stay most of the time intact rather than that they disappear completely at the end of the collapse, which is the situation simulated by the current RANS method.

Though there is a discrepancy in the quantity and extent of the vapor structures, the observed collapse behavior qualitatively matches the experimental observations.

ASSESSMENT OF CAVITATION EROSION

Paint Erosion Test

For the NACA0015 hydrofoil at 8° angle of attack (Van Rijsbergen and Boorsma, 2011 [10]), the erosion result that is recorded after re-application of the paint and two observation runs (No. 26 and 27) is shown in Figure 5. It is suggested that the high impacts can be mainly attributed to two types of events:

- The collapse of the substructures that are separated from the main sheet cavity, see the regions in white circles,
- and the collapse of the primary cloudy cavity directly shed from the main sheet cavity, related to the damaged area in red circle.

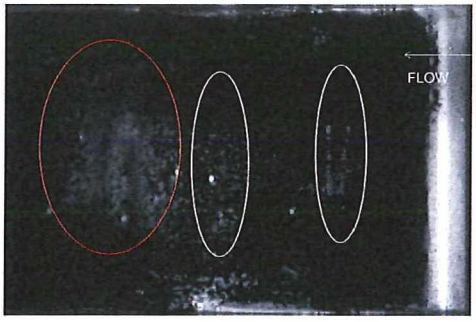

Figure 5: Paint test result after re-application of paint and run No.26 and 27 ($\sigma = 2.01, U = 17.3 m/s$) on a NACA0015 hydrofoil at 8° angle of attack (30 – 60 minutes)

Rationale behind the evaluation

From an energy consideration, it is suggested that the process of focusing of potential energy that is contained in a macro cavity may lead to high values of the impact loads, which are supposed to be related to the impulsive pressure pulses produced during the break-up and collapse process.

The potential energy E_{pot} of the macro cavity at the start of the collapse can be written as (see also Bark et al., 2004 [5]):

$$E_{pot} = V_v(p - p_v) \tag{10}$$

where V_v is the total vapor volume of the macro cavity, and p and p_v are the surrounding pressure and the vapor pressure.

Since it is not the energy that determines the erosion intensity, but rather the energy per unit time that is converted from potential energy into acoustic energy, it is the potential power that forms the basis of cavitation aggressiveness (see Van Terwisga et al., 2009 [4]).

The potential power P_{pot} can then be written as follows:

$$P_{pot} = \frac{\partial E_{pot}}{\partial t} = \frac{\partial V_v}{\partial t}(p - p_v) + V_v \frac{\partial p}{\partial t} \tag{11}$$

The above equation suggests that the instantaneous pressure p and its time derivative $\partial p / \partial t$, and the total vapor volume V_v and its time derivative $\partial V_v / \partial t$ could determine the erosive risk factors. To qualitatively assess the risk of cavitation erosion, the evaluations are mainly focusing on the local field which could be taken as the final consequence of the global unsteady dynamics on the foil surface. Based on previous work for the evaluation of various assessment criteria [17], the variation of the local pressure in time $\partial p / \partial t$ is selected to be the criterion for the assessment of regions with high erosion risk on a NACA0015 hydrofoil at 8° angle of attack.

Rate of Pressure Rise

The rate of pressure rise ($\partial p / \partial t$) over the NACA0015 hydrofoil at the intervals between the six specific instants shown in Figure 1 is examined in this section. It should be noted that the partial differential is estimated by using the first-order backward difference method:

$$\left.\frac{\partial p}{\partial t}\right|_{t+\Delta t} = \frac{p|_{t+\Delta t} - p|_t}{\Delta t} \tag{12}$$

Two adjacent instants in time will therefore be involved for each maximum value of $\partial p / \partial t$ and will be analyzed to explore the correlation between the high variation in time of the pressure and the unsteady phenomena.

Contours of the time derivative of the instantaneous local pressure ($\partial p / \partial t$) are compared with the contour plots of the instantaneous vapor volume fraction of $\alpha = 0.1$ at the relevant time points. It can be observed that the maximum value of $\partial p / \partial t$ observed during the interval between instant ② and ③ and the interval between instant ⑤ and ⑥ are found to be qualitatively in agreement with the high impacts observed in the paint erosion test, as shown in Figure 6.

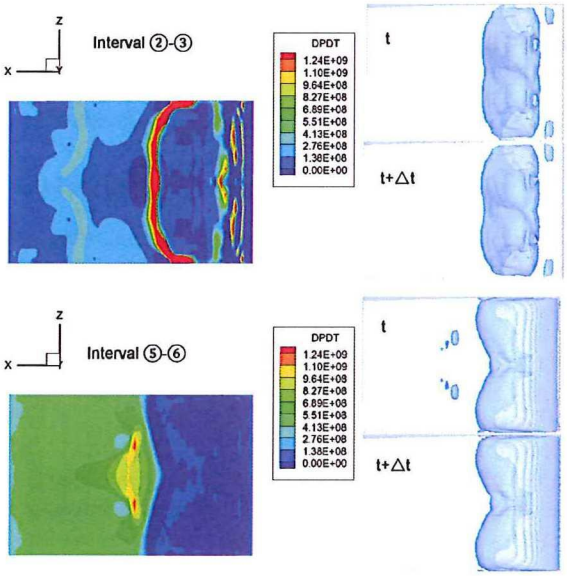

Figure 6: Contours of $\partial p / \partial t$ at the moment when its maximum value is observed for two intervals and corresponding plots of the vapor volume fraction with an iso-value of $\alpha = 0.1$ at the relevant time points

The following observations are made:

- Interval between instant ② and ③: The maximum value of $\partial p / \partial t$ is around $1.21e+10$ and occurs in the vicinity of sidewalls where the cavity disappears. High values are also observed in the area surrounding the cylindrical cavity especially in the closure region.
- Interval between instant ⑤ and ⑥: Relatively high values of $\partial p / \partial t$ can be observed at the center where the horse-shoe cloudy cavity eventually collapses. The value of the maximum pressure time derivative is however one order smaller than the $\partial p / \partial t$ value in the first time interval, causing a broad response downstream of the horse-shoe shaped cavity.

The highest value of $\partial p / \partial t$ during the whole cycle is observed between instant ① and ②. It occurs when the remaining leading edge sheet cavity begins to collapse and disappears from the leading edge, but no damage is observed near the leading edge of the hydrofoil in the paint test. However, the damaged region that is associated with high impacts can be successfully related to areas with large values of $\partial p / \partial t$ which are associated with the collapse of the substructures separated from the main sheet cavity and the horse-shoe shaped cavity. Moreover, the erosion damage located close to the sidewalls as recorded by the paint tests is also successfully captured from an analysis of $\partial p / \partial t$.

Erosion Intensity Function

It can be argued that erosion damage is not only dependent on one maximum value, but that it is a cumulative loading effect on the material, as already suggested by Hammitt (1979) [18]. For this reason, it seems better if we take the accumulated rate of pressure rise ($\partial p / \partial t$) for those values higher than a critical threshold value. This cumulative erosion intensity would thus not point toward the locations that are suffering from isolated peaks in pressure gradient only.

Therefore, an erosion intensity function is proposed:

$$I_{Erosion} = \frac{1}{N}\sum I_i \quad and \quad I_i = \begin{cases} \dfrac{\partial p}{\partial t}; & \dfrac{\partial p}{\partial t} \geq Threshold \\ 0; & \dfrac{\partial p}{\partial t} < Threshold \end{cases} \qquad (13)$$

where the subscript i refers to each individual time instant, determined by the selected time step size. N is the number of the events with a value of $\partial p / \partial t$ higher than a certain threshold level.

Due to a lack of knowledge on the material properties of the foil's surface coating, a series of thresholds are applied to equation (13) for the evaluation of erosion intensity. It is found that when the threshold level becomes higher than a value in the order of $4e+09$, the damage caused by the collapse of the horse-shoe shaped vapor structures will not be captured. A minimum level of the threshold level is found to be $1e+08$ so as to avoid a situation that a high erosion risk is indicated over the complete hydrofoil.

Compared with the experimental results, the erosion intensity calculated with a threshold level of $3e+09$ is found to best correlate with the damage regions observed from the paint test, as shown in Figure 7.

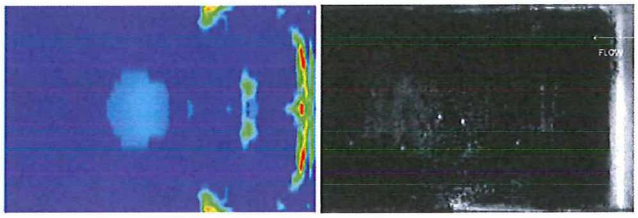

(a) Numerical results (b) Results from paint tests

Figure 7: Comparison between (a) a high erosion risk predicted by equation (13) with a threshold value of $3e+09$ and (b) the damage area observed from paint tests (Foil: NACA0015, AoA=8°; flow from right to left)

The discrepancies between the results from the erosion intensity function $I_{Erosion}$ and the experimental observations can be ascribed to the discrepancies in the locations of the collapses of the shed cloudy cavity and the far smaller structures in the chord-wise direction between the numerical results and the experimental observations. It can be concluded that the erosion intensity function $I_{Erosion}$ provides a better criterion to assess the cavitation erosion risk than the time derivative of local pressure $\partial p / \partial t$. An appropriate threshold level for the initial accumulation is critical for the final results, which is supposed to depend on the material properties only.

CONCLUSIONS

It is concluded from this study that:

- A realistic dynamic shedding of the sheet cavitation is only obtained after attenuating the eddy viscosity in the region with higher vapor volume fractions in the multiphase RANS method implemented in FLUENT. It seems that the modified turbulence model is less dissipative, thereby avoiding too much energy dissipation in the highly unsteady flow.
- Due to the effect of the vertical side wall boundary layer, the re-entrant jet can be observed not only to move in upstream direction, but also to move towards the mid-span. It is believed that this wall effect is an important reason for the horse-shoe shaped cloudy cavity to develop.
- An encouraging correlation is found between the damaged regions from the paint tests and the areas with a large value of the time derivative of the local pressure $\partial p / \partial t$.
- A newly proposed erosion intensity function (equation(13)) is based on the mean of peak values of the time derivative of the local pressure $\partial p / \partial t$ that exceeds a certain threshold. This function gives the best correspondence between the locations with the highest erosion risk from the computations and the damage areas obtained from the experiments. Further validation studies are recommended for this erosion intensity function.

ACKNOWLEDGEMENT

The authors are grateful for the reports of the experiments on the NACA0015 hydrofoil provided by the Cooperative Research Ships (CRS), administered by MARIN. Experimental data on the NACA0015 hydrofoil have been made available by the Cavitation Erosion Project of CRS.

NOMENCLATURE

C	Chord Length of the hydrofoil	mm
E_{pot}	Potential energy	kgm^2s^{-2}
$I_{Erosion}$	Erosion intensity	$kgm^{-1}s^{-3}$
I_i	i^{th} individual intensity	$kgm^{-1}s^{-3}$
k	Turbulence kinetic energy	m^2s^{-2}
n_b	Bubble number density	m^{-4}
N	Number of events	
p	Local mixture pressure	$kgm^{-1}s^{-2}$
p_v	Vapor pressure	$kgm^{-1}s^{-2}$
P_{pot}	Instantaneous potential power	kgm^2s^{-3}
R	Bubble radius	m
S_e	Evaporation of the vapor bubbles	
S_c	Condensation of the vapor bubbles	
u	Velocity of the mixture	ms^{-1}
V_v	Vapor volume	m^3
y^+	Non-dimensional wall distance	
α	Vapor volume fraction	
ε	Dissipation rate of turbulent kinetic energy	m^2s^{-3}
μ_t	Turbulent viscosity	
$\rho_{m,l,v}$	Mixture, liquid and vapor density	kgm^{-3}
σ	Cavitation Number	
ω	Specific dissipation rate of turbulent kinetic energy	s^{-1}

REFERENCES

[1] Fortes-Patella, R., Reboud, J.L. and Briancon-Marjollet, L. 2004, "A phenomenological and numerical model for scaling the flow aggressiveness is cavitation erosion," *EROCAV Workshop*, Val de Reuil.

[2] Dular, M., Sirok, B. and Sroffel, B. 2006, "Experimental and numerical modelling of cavitation erosion," *6th International Symposium on* Cavitation, *CAV2006,* Wageningen.

[3] Nohmi, M. Iga, Y., and Ikohagi, T. 2008, "Numerical prediction of cavitation erosion," *Proceeding of FEDSM2008*, Jacksonville, Florida USA.

[4] Van Terwisga, T.J.C., Fitzsimmons, P.A., Ziru Li, and Foeth, E.J. 2009, "Cavitation Erosion – A review of physical mechanisms and erosion risk models," *CAV2009,* Ann Arbor, USA.

[5] Bark, G., Berchiche, N. and Grekula, M. 2004, "Application of principles for observation and analysis of eroding cavitation - The EROCAV observation handbook, " *Edition 3.1.*

[6] Reboud J. L., Stutz B and Coutier O. 1998, "Two phase flow structure of cavitation experiment and modeling of unsteady effects," *Proceedings of the 3rd International Symposium on Cavitation*, Grenoble, France, 1998.

[7] Oprea, I. 2009, "Wärtsilä CFD results: 2D NACA0015 foil," *Virtue WP4 Workshop*, Wärtsilä.

[8] Hoekstra, M. and Vaz, G. 2008, "FreSCo exercises for NACA0015 foil," *Virtue WP4 Workshop*, MARIN.

[9] Hoekstra, M., Van Terwisga, T.J.C. and Foeth, E.J. 2011, "smp'11 Workshop-Case 1: DelftFoil," *2nd International Symposium on Marine Propulsors*, Hamburg, Germany.

[10] Van Rijsbergen, M. and Boorsma, A. 2011, "High speed video observations and acoustic impact measurements on a NACA0015 foil," *CRS EROSION II Working Group, proprietary.*

[11] Menter, F.R. 1994, "Two-equation eddy-viscosity turbulence models for engineering applications," *AIAA Journal.*

[12] ANSYS, Inc. 2009, *FLUENT Theory Guide (Release 12.0).*

[13] Li, Z.R., Pourquie, M. and Van Terwisga, T.J.C. 2011, "On the assessment of cavitation erosion on a hydrofoil using unsteady RANS," *WIMRC 3rd International Cavitation Forum 2011*, University of Warwick, UK.

[14] Kawanami,Y., Kato, H., Yamaguchi, H., Maeda, M. and Nakasumi, S. 2002, "Inner structure of cloud cavity on a foil section," *JSME International Journal*, 45 (3), 655-661.

[15] Saito, Y. Y., Takami, R., Nakanori, I. and Ikohagi, T. 2007, "Numerical analysis of unsteady behavior of cloud cavitation around a NACA0015 foil," *Computational Mechanics*, 40, 85-96.

[16] Boorsma, A. 2010, "Cavitation tests on a NACA0015 aerofoil – Quantification of cavitation impacts from high speed video and AE signals," *CRS EROSION II Working Group.*

[17] Li, Z.R. 2012, "Assessment of cavitation erosion with a multiphase Reynolds-Averaged Navier-Stokes method," *PhD Thesis, TUDelft.*

[18] Hammitt, F.G. 1979, "Cavitation erosion state of art and predicting capability," *Applied Mechanics Review, ASME.*